Pseudo-easy-axis anisotropy in antiferromagnetic $S = 1$ diamond-lattice systems

S. Vaidya,[1,2,*] A. Hernández-Melián,[3] J. P. Tidey,[1] S. P. M. Curley,[1] S. Sharma,[1] P. Manuel,[4] C. Wang,[5] G. L. Hannaford,[3] S. J. Blundell,[6] Z. E. Manson,[7] J. L. Manson,[7,†] J. Singleton,[8] T. Lancaster,[3] R. D. Johnson,[9,10] and P. A. Goddard[1,‡]

[1]*Department of Physics, University of Warwick, Gibbet Hill Road, Coventry CV4 7AL, United Kingdom*
[2]*School of Physics & Astronomy, University of Birmingham, Edgbaston, Birmingham B15 2TT, United Kingdom*
[3]*Department of Physics, Durham University, South Road, Durham DH1 3LE, United Kingdom*
[4]*ISIS Pulsed Neutron Source, STFC Rutherford Appleton Laboratory, Didcot, Oxfordshire OX11 0QX, United Kingdom*
[5]*Laboratory for Muon Spin Spectroscopy, Paul Scherrer Institute, 5232 Villigen, Switzerland*
[6]*Department of Physics, Clarendon Laboratory, University of Oxford, Parks Road, Oxford OX1 3PU, United Kingdom*
[7]*Department of Chemistry and Biochemistry, Eastern Washington University, Cheney, Washington 99004, USA*
[8]*National High Magnetic Field Laboratory (NHMFL), Los Alamos National Laboratory, Los Alamos, New Mexico 87545, USA*
[9]*Department of Physics and Astronomy, University College London, Gower Street, London WC1E 6BT, United Kingdom*
[10]*London Centre for Nanotechnology, University College London, London WC1H 0AH, United Kingdom*

(Received 24 May 2024; accepted 10 October 2024; published 21 November 2024)

We investigate the magnetic properties of $S = 1$ antiferromagnetic diamond-lattice, $NiX_2(\text{pyrimidine})_2$ (X = Cl, Br), hosting a single-ion anisotropy (SIA) orientation which alternates between neighboring sites. Through neutron diffraction measurements of the X = Cl compound, the ordered state spins are found to align collinearly along a pseduo-easy axis, a unique direction created by the intersection of two easy planes. Similarities in the magnetization, exhibiting spin-flop transitions, and the magnetic susceptibility in the two compounds imply that the same magnetic structure and a pseduo-easy axis is also present for X = Br. We estimate the Hamiltonian parameters by combining analytical calculations and Monte Carlo (MC) simulations of the spin-flop and saturation field. The MC simulations also reveal that the spin-flop transition occurs when the applied field is parallel to the pseduo-easy axis. Contrary to conventional easy-axis systems, there exist field directions perpendicular to the pseduo-easy axis for which the magnetic saturation is approached asymptotically and no symmetry-breaking phase transition is observed at finite fields.

DOI: 10.1103/PhysRevB.110.174438

I. INTRODUCTION

A fundamental goal in condensed matter physics has been the control of dominant energy scales in magnetic systems, allowing experimental exploration of various emergent phases and quantum phenomena. To this end, molecule-based magnets, where molecular ligands link magnetic metal ions, have proven particularly effective [1–5]. The wide choices of ligands available provide a high level of control over the final crystal structure and thus control over various aspects of the magnetic properties [6–8]. For example, a mix of bridging and nonbridging ligands can be used to create quasi-low-dimensional magnetic structures [9–11]. The control over the magnetic properties has been achieved through various means, including the substitution of ligands [12–17], metal-ions [10,18] and counter-ions [19,20], and by applying hydrostatic pressure [21–24]. Moreover, organic ligands such as pyrimidine (pym = $C_4H_4N_2$) provide the flexibility to create structurally nontrivial systems such as staggered and chiral antiferromagnetic (AFM) $S = 1/2$ spin chains [25–28]. In these systems, the alternating orientation of the spin octahedra between nearest neighbors leads to magnetic properties that differ significantly from conventional spin-half chains. Such properties were explained by the application of the sine-Gordon model of quantum field theory [29,30].

In the present study, we explore the effects of halide substitution and alternating local octahedra orientation in the context of $S = 1$ three-dimensional diamond-lattice systems $NiX_2(\text{pym})_2$, where X = Cl, Br. The zero-field-splitting in these systems presents the possibility of single-ion-anisotropy (SIA), with energy D, which follows the local spin octahedra and alternates in orientation on neighboring spin sites. Previous studies on the isostructural $S = 2$ system $FeCl_2(\text{pym})_2$, showed that an alternating easy-axis SIA direction results in a large canting angle of 14° and weak ferromagnetism significantly larger than that which is conventionally caused by the Dzyaloshinskii-Moriya (DM) interaction alone [31]. A subsequent study on $NiCl_2(\text{pym})_2$ under applied hydrostatic pressure observed temperature-dependent magnetic susceptibility, $\chi(T)$, curves that exhibited similarities to the $\chi(T)$ of $FeCl_2(\text{pym})_2$. This led to the assumption that the Ni system hosted a similar spin-canted ground state [32]. However,

*Contact author: s.vaidya@warwick.ac.uk
†Deceased.
‡Contact author: p.goddard@warwick.ac.uk

neutron diffraction or magnetic hysteresis measurements showing a zero-field remanent magnetization were not available to support this claim. The application of pressure was reported to increase the magnetic ordering temperature, T_N, due to increasing orbital overlap in the Ni–N (N from the pym) bond. Quantitative modeling of the pressure-dependent T_N found that $J \approx 7$ K but an estimation for the size of the SIA was not possible. More recently, studies on a family of metal-organic magnets MCl_2L, where $M =$ Ni and Fe, $L =$ (pym) and 2,1,3-benzothiadiazole (btd) also find that an alternating easy axis induces a canted magnetic structure [33]. In contrast, in the frustrated chain-like material, Cs_2CoBr_4, easy-plane anisotropy, alternating between weakly coupled chains, led to the formation of collinear magnetic order [34,35].

Our neutron diffraction measurements reveals a collinear magnetic structure in $NiCl_2(pym)_2$, which is attributed to an *easy-plane* SIA that alternates in orientation. The intersection of these alternating planes coupled with the nearest-neighbor antiferromagnetic exchange interaction creates a unique pseudo-easy axis along which the moments align. Given the similarities in the crystal structures (determined using electron diffraction), magnetometry, and muon-spin rotation (μ^+SR) data, we propose that a pseudo-easy axis is also present in the $X =$ Br case. The magnetic order present in these systems is consistent with the negligible zero-field remanent magnetization in measurements of the field-dependent magnetization, $M(H)$. Additionally, we find that the pseudo-easy axis, similar to a real easy axis, results in a spin-flop transition seen in the $M(H)$ data. Monte Carlo (MC) simulations of $M(H)$ and mean-field calculations of the spin-flop and saturation field, H_{SF} and H_{C1}, respectively, are used to determine J and D for $X =$ Cl and Br. For $X =$ Br, we find that D is reduced while a secondary AFM interaction mediated by the $X \cdots X$ exchange bonds is increased. This is in keeping with the trends established in the magnetic chain compounds $NiX_2(3,5\text{-lut})_4$ ($X =$ HF2, Cl, Br, or I) [17] and $NiX_2(pyz)_2$ (pyz = pyrazine $C_4H_4N_2$; $X =$ Cl, Br, I, NCS) [15]. Finally, MC simulations of single-crystal $M(H)$ curves reveal that a magnetic saturation phase transition only occurs for fields applied along certain directions.

II. RESULTS AND DISCUSSION

A. Crystal structure

The crystal structures of both $X =$ Cl and Br compound are solved using single-crystal electron diffraction (3D ED) at $T = 120$ K with lattice parameters obtained from powder x-ray diffraction (PXRD) measurements collected at the I11 beamline of the Diamond Light Source at the same temperature. The details of these measurements and the structural refinement can be found in the Supplemental Material [36]. The resulting crystal structure of $NiX_2(pym)_2$ is illustrated in Fig. 1 and Table I provides the lattice parameters.

The $X =$ Cl and $X =$ Br materials are isostructural and both crystallize in the $I4_122$ space group. These materials consist of three-dimensional diamond-like networks of Ni(II) ions connected by the pym ligand. The Ni(II) ions sit at the center of axially distorted octahedra consisting of four equatorial bonds to the N atoms of the pym rings and two longer axial coordination bonds to the halides.

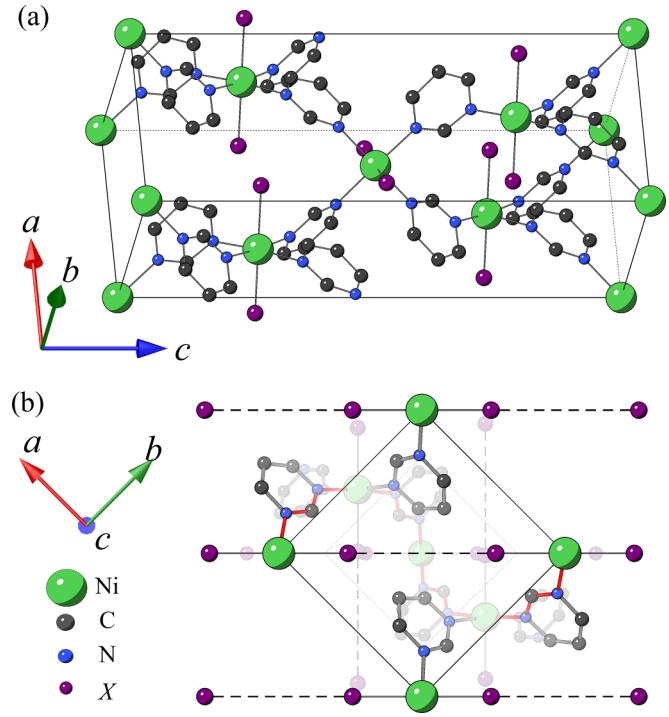

FIG. 1. (a) The $I4_122$ crystal structure of $NiX_2(pym)_2$ where $X =$ Cl or Br and pym = pyrimidine. (b) Displays the view down the c-axis. In this structure, the pym ligands bridge neighboring Ni ions and mediate the primary exchange interaction, forming a three-dimensional diamond network. Between neighboring Ni ions connected by pym, the Ni–X axial bond direction rotates by 90°. The black-dashed lines highlight the weak $X \cdots X$ exchange bonds that mediate the secondary exchange interaction along the Ni–$X \cdots X$–Ni chains. The red bond highlights the exchange pathway, in the Ni–pym network, between two Ni(II) ions connected by the $X \cdots X$ exchange bond.

Within the unit cell Ni(II) ions reside in planes perpendicular to c at heights of $z = 0$, $c/4$, $c/2$, and $3c/4$. For Ni(II) ions in the $z = 0$ and $z = c/2$ planes, the axial direction of the local octahedra is orientated along the $[\bar{1}\,1\,0]$ direction. Owing to the 4_1 screw symmetry, this axial direction is rotated by 90° to align along [1 1 0] for Ni(II) ions in the $z = c/4$ and $z = 3c/4$ planes. This rotation ensures if a SIA anisotropy is present in these systems it will be rotated by 90° between neighboring spins connected by pym.

Pym ligands have been shown to be an effective mediator of exchange interactions of the order of 10 K [33]. Secondary interactions are mediated through the halide-halide exchange bond, shown as dashed lines in Figs. 1(a) and 1(b). Such exchange paths depend strongly on the halide ions, but are known to carry exchange of the order of 1 K [17]. This

TABLE I. Lattice parameters for the $I4_122$ structure of $NiX_2(pym)_2$, $X =$ Cl and $X =$ Br, determined using powder x-ray diffraction at $T = 120$ K.

	a, b (Å)	c (Å)
$NiCl_2(pym)_2$	7.3576(2)	19.4956(5)
$NiBr_2(pym)_2$	7.50690(6)	19.5378(2)

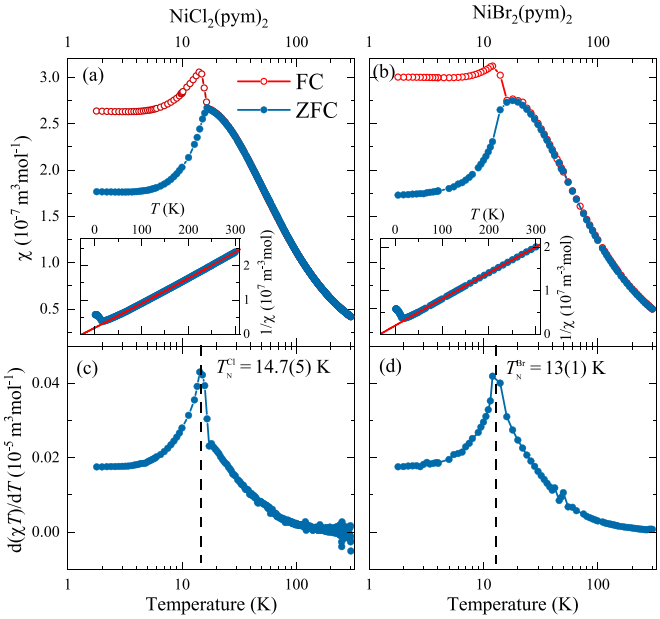

FIG. 2. Temperature-dependent magnetic susceptibility $\chi(T)$ for powder samples of NiX_2(pym)$_2$, where (a) $X =$ Cl and (b) $X =$ Br. For both a field of $\mu_0 H = 0.1$ T was applied, the field-cooled data are depicted as red circles and zero-field-cooled (ZFC) data are blue circles. The insets present the Curie-Weiss fit to the ZFC χ^{-1}. (c), (d) Peak in the ZFC $\mathrm{d}(\chi T)/\mathrm{d}T$ marks the onset of magnetic long-range order at $T_N = 14.7(5)$ K for $X =$ Cl and $T_N = 13(1)$ K for $X =$ Br.

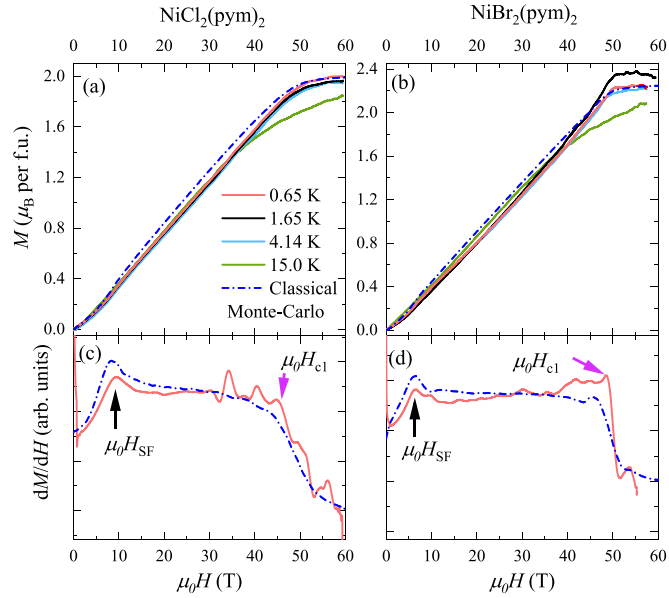

FIG. 3. Powder-averaged magnetization, $M(H)$, data for NiX_2(pym)$_2$, where (a) $X =$ Cl and (b) $X =$ Br at various temperatures. The $T = 0.65$ K differential susceptibility, $\mathrm{d}M/\mathrm{d}H$, below ordering temperature for (c) $X =$ Cl and (d) $X =$ Br. The black arrows mark the spin-flop field in both and the blue dash-dotted lines show the results of the classical Monte Carlo simulation discussed in Sec. II E of the text.

results in weakly interacting Ni–$X\cdots X$–Ni chains propagating along the $[\bar{1}\,1\,0]$ direction for ions in the $z = 0$ and $z = c/2$ planes and along $[1\,1\,0]$ for ion in the $z = c/4$ and $z = 3c/4$ planes. In the cases where there is AFM coupling through both the pym ligands and the halide-halide exchange bonds, the two interactions will be in competition, resulting in a reduced net effective interaction.

The spin Hamiltonian of NiX_2(pym)$_2$, written in terms of the two spin sites i and j is

$$\mathcal{H} = J\sum_{\langle i,j\rangle}\mathbf{S}_i\cdot\mathbf{S}_j + \sum_{(i,j)} g\mu_B\mu_0\mathbf{H}\cdot\mathbf{S}_{i,j} + D\left[\sum_i(\hat{\mathbf{D}}_i\cdot\mathbf{S}_i)^2 + \sum_j(\hat{\mathbf{D}}_j\cdot\mathbf{S}_j)^2\right]. \quad (1)$$

Here, $\mathbf{S}_{i,j}$ is the spin of each ion, $\langle i, j\rangle$ denotes the sum over unique pairs of neighboring spins with exchange interaction strength J, D is the size of the SIA, $\hat{\mathbf{D}}_i = [\bar{1}10]/\sqrt{2}$, and $\hat{\mathbf{D}}_j = [110]/\sqrt{2}$ are the hard-axis unit vectors for sites i and j, and $g\mu_B\mu_0\mathbf{H}\cdot\mathbf{S}_{i,j}$ is the Zeeman energy term assuming an isotropic g-factor. Although the symmetry permits the DM interaction, its magnitude is expected to be small compared to the terms in Hamiltonian given in Eq. (1). As we will show in the following sections, all data presented here can be accounted for by this minimal Hamiltonian.

B. Magnetometry

Powder $\chi(T)$ data for $X =$ Cl are presented in Fig. 2(a). On cooling from 300 K, both the field-cooled (FC) and zero-field-cooled (ZFC) data exhibit a smooth rise to a sharp cusp and a bifurcation of the two curves at $T \approx 15$ K. Plotting the ZFC data as $\mathrm{d}(\chi T)/\mathrm{d}T$ in Fig. 2(d) reveals a lambda-like peak, close to the bifurcation, which is suggestive of a transition to long-range magnetic order below $T_N = 14.7(5)$ K [37]. Further cooling results in plateaus in the FC and ZFC curves below 4.6 K. In the inset to Fig. 2(a), a Curie-Weiss (CW) fit to the inverse susceptibility, $\chi(T)^{-1}$, for 50 K $\leqslant T \leqslant$ 300 K, yields $g = 2.14(1)$, CW temperature $\theta_{CW} = -26.1(2)$ K, and a temperature-independent constant $\chi_0 = -2.62(5)\times10^{-9}$ m^{3}mol^{-1}. The negative θ_{CW} here indicates an AFM coupling of the Ni ions.

The $\chi(T)$ curves for $X =$ Br in Fig. 2(b) display a similar behavior to $X =$ Cl. However, the bifurcation and the lambda peak in ZFC $\mathrm{d}(\chi T)/\mathrm{d}T$ [see Fig. 2(d)] are suppressed to a lower $T_N = 13(1)$ K, revealing a rounded local maximum prior to the bifurcation of the ZFC and FC curves. CW fit to the $\chi(T)^{-1}$ [see inset to Fig. 2(b)], results in $g = 2.27(1)$, $\theta_{CW} = -31.7(2)$ K, and $\chi_0 = 1.09(9)\times10^{-9}$ m^{3}mol^{-1}.

Figures 3(a) and 3(b) present the pulsed-field $M(H)$ data for $X =$ Cl and Br, respectively. In both materials, at low fields and temperatures below T_N, there is an upturn in the magnetization observed as a peak in the differential susceptibility, $\mathrm{d}M/\mathrm{d}H$, shown in Figs. 3(c) and 3(d). These features, reminiscent of the spin-flop transition found in easy-axis systems, are observed at $\mu_0 H_{SF} = 9.5(8)$ T and 6.6(8) T for $X =$ Cl and Br, respectively. In the $X =$ Cl sample, further increase in field results in a near linear rise in $M(H)$, up to the first saturation field $H_{c1} = 46(3)$ T. H_{c1} is defined as the point where $M(H)$ deviates from a linear field dependence (point where $\mathrm{d}M/\mathrm{d}H$ starts to decrease). The 0.65 K $M(H)$ data for

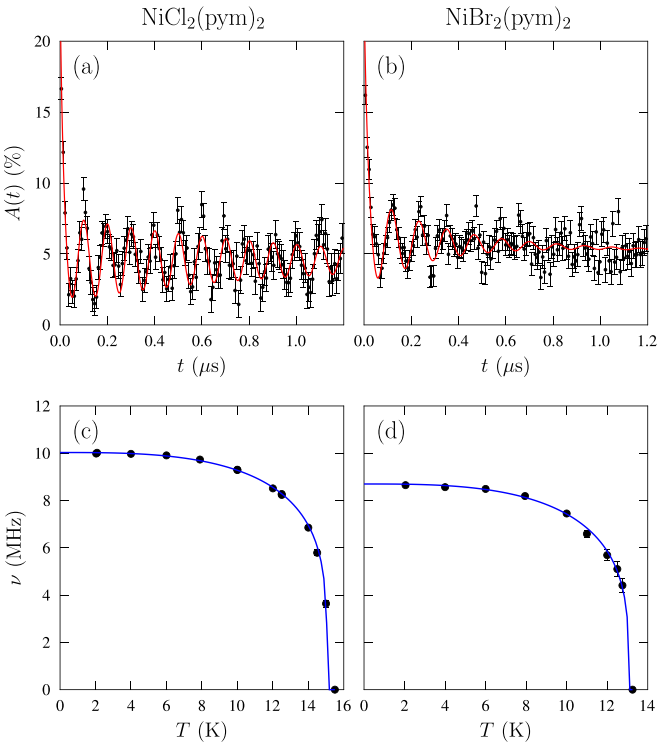

FIG. 4. The zero-field μ^+SR spectra data (black circles) collected at $T = 4$ K for NiX_2(pym)$_2$, where (a) $X =$ Cl and (b) $X =$ Br. The temperature dependence of the oscillation frequency ν for (c) $X =$ Cl and (d) $X =$ Br. The solid lines represent fits to the data.

$X =$ Br display a slightly concave approach to the first saturation field, resulting in a peak in dM/dH at $H_{c1} = 48(1)$ T. As we will show in Sec. II E, H_{c1} corresponds to magnetic saturation for grains in which the field aligns along the [0 0 1] axis. For $H > H_{c1}$, the projected value of the saturation magnetization suggests a low-temperature g factor of $g = 2.06$ for $X =$ Cl and $g = 2.25$ for $X =$ Br. The g for $X =$ Cl is slightly lower than predicted by the CW fit at high temperatures while the values for $X =$ Br are in good agreement.

For a spin-canted magnetic structure, similar to FeCl$_2$(pym)$_2$, a remanent $M(H)$ at zero-field is expected. However, in both $X =$ Cl and Br, very small remanent $M(0)$ of 0.001 μ_B and 0.00016 μ_B per Ni(II) ion, respectively, are observed [36]. These small $M(0)$ are readily explained by the presence of a small amount of NiX_2(pym) impurity phases (as seen in the crystallographic data for the $X =$ Cl sample in the Supplemental material [36]) which are known to exhibit a $M(0) = 0.127$ μ_B per Ni(II) [33].

C. Muon-spin rotation

Zero-field μ^+SR measurements were carried out at the Swiss Muon Source, Paul Scherrer Institut. Data were collected at temperatures $2 \leqslant T \leqslant 16$ K and example spectra at 4 K for $X =$ Cl and $X =$ Br are shown in Figs. 4(a) and 4(b), respectively. For both materials, the time-dependent asymmetry function exhibits clear oscillations, indicative of long-range magnetic order throughout the bulk of the material. The quasistatic local field, arising in the presence of long-range magnetic order, causes a coherent precession of the spin of those muons for which a component of their spin polarization lies perpendicular to this local field (expected to be 2/3 of the total spin polarization for a polycrystalline sample). The frequency of the oscillation is given by $\nu_i = \gamma_\mu |B_i|/2\pi$, where $\gamma_\mu = 2\pi \times 135.5$ MHz T^{-1} is the muon gyromagnetic ratio and B_i is the average magnitude of the local magnetic field at the i^{th} muon site. As such, ν_i is an effective order parameter and indicative of the total ordered moment within each sample.

To describe the temperature evolution of the asymmetry function and hence $\nu_i(T)$, fits were produced to a function of the form

$$A(t) = A_1 e^{-\lambda_1 t} \cos(2\pi \nu t) + A_2 e^{-\lambda_2 t} + A_b, \tag{2}$$

where λ_i are relaxation rates and A_b is a background contribution from muons stopping outside the sample. The first term in Eq. (2) accounts for the oscillatory signal and the second term accounts for the muon polarization initially parallel to the local magnetic field. The presence of a single frequency for both materials implies that a single muon site gives rise to the oscillatory components of the spectra. The resulting temperature-dependent $\nu(T)$, shown in Figs. 4(c) and 4(d), is described using the phenomenological function [38]

$$\nu(T) = \left[1 - \left(\frac{T}{T_N}\right)^{\alpha}\right]^{\beta}. \tag{3}$$

For $X =$ Cl, we obtain $\nu(0) = 10.0(1)$ MHz (corresponding to a local field of 74 mT), $T_N = 15.05(1)$, and $\beta = 0.22(1)$ for a fixed $\alpha = 3$. The ordering temperature extracted here is in excellent agreement with the analysis of the $\chi(T)$ data. The rapid drop in $\nu(T)$ with increasing temperature along with the fitted value of β implies the existence of fluctuations, close to the phase transition, that are intermediate between a two- and three-dimensional character. For $X =$ Br, the fit yields $\nu(0) = 8.70(3)$ MHz (corresponding to a local field of 64 mT), $T_N = 13.1(1)$, and $\beta = 0.27(1)$. The ordering temperature is again in excellent agreement with the $\chi(T)$ data. Compared to $X =$ Cl, an increased β in $X =$ Br implies the fluctuations here are more three-dimensional. This is in keeping with the expectation that there are nonzero exchange interactions through the halides in the $X =$ Br system, while in $X =$ Cl this interaction is expected to be much smaller [17].

D. Elastic neutron scattering

Elastic neutron diffraction measurements on powder samples of NiCl$_2$(pym)$_2$ were performed on the WISH instrument at the ISIS, UK Neutron and Muon Source [39], at temperatures above ($T = 20$ K) and below ($T = 1.4$ K) the magnetic ordering transition. Rietveld refinement of the nuclear structure was performed on the data collected at $T = 20$ K, across four separate detector banks, using the FULLPROF software package [40]. Figure 5(a) present the structural fit with $R_{Bragg} = 3.361\%$ to data from one such detector bank at average $2\theta = 58.330^\circ$. The resulting lattice parameters, $a = 7.3425(2)$ Å and $c = 19.4841(9)$ Å, and nuclear structure are in good agreement with the values determined from the 3D ED and PXRD measurements at 120 K and accounted for all observed peaks at 20 K.

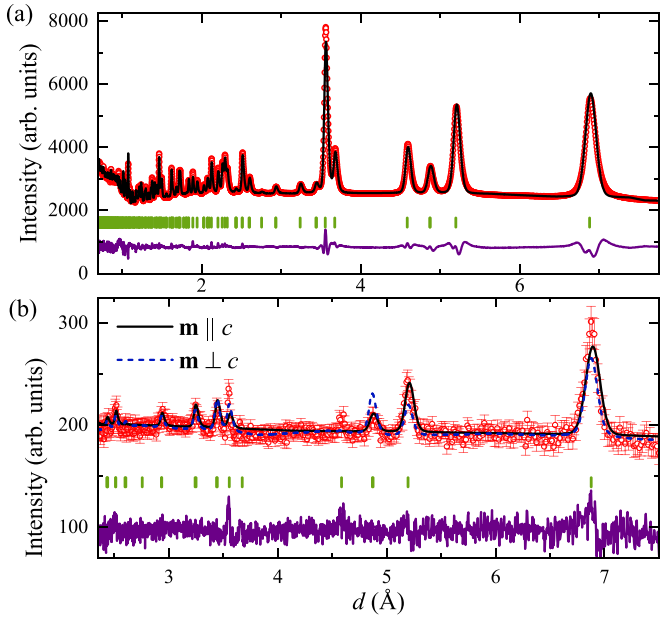

FIG. 5. (a) Rietveld refinement of the $I4_122$ the nuclear structure of $NiCl_2(pym)_2$ to powder neutron diffraction data collected at $T = 20$ K. The data points are shown as red circles, fitting curve in black, Bragg positions are marked by green ticks, and the difference between the data and the calculated pattern is shown in purple. (b) Magnetic diffraction pattern obtained by subtracting data collected at 20 K from the 1.4 K data. The fitted pattern (black) has magnetic moments parallel to the c-axis compared to the pattern with moments perpendicular to c (blue dashed line).

The difference between the data collected at $T = 1.4$ K and $T = 20$ K reveals magnetic Bragg peaks residing on top of the nuclear peak positions, indicating magnetic order with propagation vector $\mathbf{k} = (0, 0, 0)$. Symmetry analysis in ISODISTORT [41,42] reveals three candidate symmetries (irreps $m\Gamma_2$, $m\Gamma_3$, and $m\Gamma_5$) for the magnetic structure. Among these, $m\Gamma_3$ corresponds to ferromagnetic (FM) order and is ruled out from the $\chi(T)$ measurements. The magnetic moments in the magnetic structure described by the $m\Gamma_2$ irrep are constrained to point parallel to the c-axis with nearest-neighbors antiferromagnetically coupled through pym. Consequently, the ordered moment size is the only refinable parameter in this irrep. The structure associated with $m\Gamma_5$ irrep decomposes into a linear combination of perpendicular FM and AFM modes within the ab-plane and hence encompasses the canted structure observed in the $FeCl_2(pym)_2$ system [31].

The diffraction pattern resulting from the refinement of both AFM models is shown in Fig. 5(b). The magnetic structure associated with irrep $m\Gamma_2$ is found to best fit the data with $R_{mag} = 4.16\%$ compared to $R_{mag} = 34.89\%$ of irrep $m\Gamma_5$. The resulting ordered moment size is 1.99(3) μ_B per Ni(II) ion, which is in excellent agreement with the low-temperature magnetic saturation value. The resulting collinear magnetic structure is depicted in Fig. 6 and is consistent with an easy-plane SIA. While the local easy plane, defined by the local Ni–pym equatorial plane and shown as blue circles in Fig. 6, rotates by 90° between each neighboring Ni(II) ion, the intersection of these planes defines a pseudo-easy axis along the

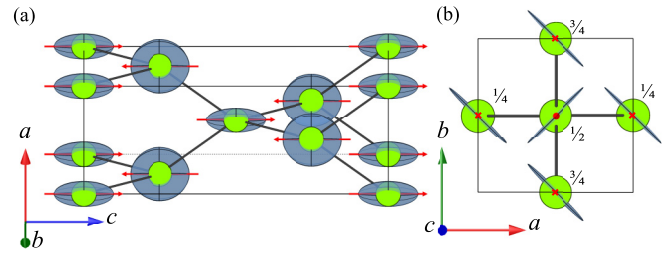

FIG. 6. (a) Zero-field magnetic structure of $NiCl_2(pym)_2$ determined through powder neutron diffraction. The red arrows indicate the magnetic moment direction of Ni(II) ions (green spheres). The blue circles show the local single-ion easy plane of Ni(II) ions and the black lines show the nearest neighbors' exchange interactions. (b) View down the c-axis illustrates 90° rotation of the easy plane between nearest neighbours. Ni(II) ions at $[x, y, 0]$ and $[x, y, 1]$ are omitted for clarity.

c direction. Moments aligning along this axis satisfy both the exchange interaction through pym and the SIA. The collinear structure observed here indicates the absence of any significant DM interaction, which would result in spin-canting. Additionally, the $\mathbf{k} = (0, 0, 0)$ vector and the magnetic structure is only possible when the exchange through the pym is dominant and AFM.

Our bulk magnetic characterisation suggests $X = Cl$ and $X = Br$ are described by the same magnetic Hamiltonians but with differing values of J and D. Since the magnetic ground state determined for $X = Cl$ is independent of the values of AFM J and easy-plane D, we expect $NiBr_2(pym)_2$ will adopt the same magnetic structure.

E. Calculations and simulations

1. Critcal fields

In a similar manner to ordinary easy-axis systems, applying the field parallel to the pseudo-easy axis will cause a spin-flop and magnetic saturation transitions which are seen in the $M(H)$ data in Fig. 3. Mean-field calculations, under the assumption that $D \ll nJ$, presented in the Supplemental Material [36], predict that these transitions occur at

$$\mu_0 H_{c1} = \frac{2nJ - D}{g\mu_B}, \tag{4}$$

$$\mu_0 H_{SF} = \frac{\sqrt{2nJD - D^2}}{g\mu_B}. \tag{5}$$

Here $n = 4$ is the number of nearest neighbors. Taking the isotropic low-temperature g-factors and the critical field from the $M(H)$ data, we determine that $J = 8.1(5)$ K, $D = 2.6(5)$ K for $X = Cl$ and $J = 9.2(2)$ K, $D = 1.2(3)$ K for $X = Br$. The phase diagram of D/J ratio against the ratio of Zeeman energy and exchange energy, $g\mu B\mu 0H/J$, is shown in Fig. 7. While the phase diagram extends up to $D/J = 1.50$ in Fig. 7, the zero-field collinear AFM order induced by the pseudo-easy-axis anisotropy may be expected to extend up to larger values of D/J. Indeed, in Cs_2CoBr_4, the collinear AFM ground state is present for $D/J \sim 8$ [34]. The D/J ratios for both $X = Cl$ and Br materials are marked in the phase diagram and are summarized in Table II.

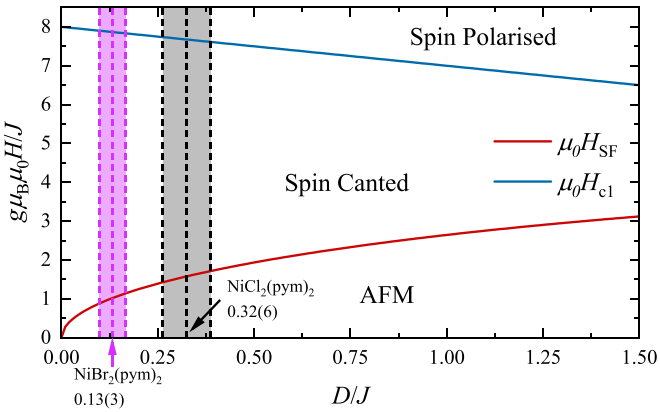

FIG. 7. Phase diagram for $NiX_2(pym)_2$, for $\mathbf{H}||c$ and calculated using a classical mean-field model described in the text. The x-axis is the ratio of easy-plane single-ion anisotropy and the exchange energies. The y-axis is the ratio of the Zeeman and the exchange energy. The red line represents the calculated spin-flop transition taking the systems from an antiferromagnetic state to a spin-canted state. The blue line is the boundary between the spin canted to the spin-polarized state. The black and purple dashed lines mark the D/J ratio of the $X =$ Cl and Br materials, respectively, and the shaded regions indicate the experimental uncertainty in these values.

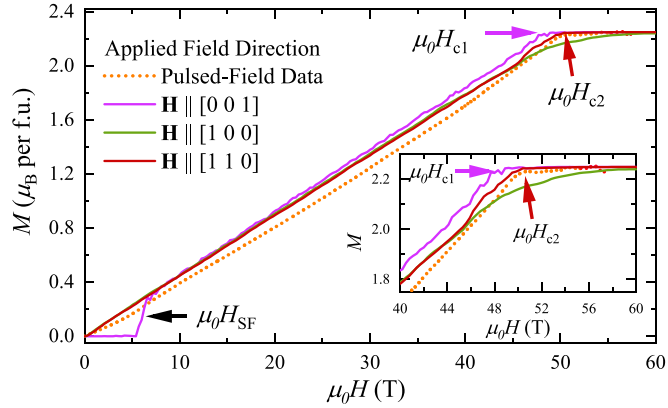

FIG. 8. Monte Carlo simulation of the magnetization $M(H)$ for $NiBr_2(pym)_2$ with the field along various crystallographic directions along with the measured pulsed field $M(H)$ data. The inset is zoomed into the $40 \leqslant \mu_0 H \leqslant 60$ T range. The black arrow highlights the spin-flop field and the purple arrow points toward the saturation field for $\mathbf{H}||[0\,0\,1]$ (field parallel to pseudo-easy axis). The red arrow indicates the saturation field for $\mathbf{H}||[1\,1\,0]$ (perpendicular to the pseudo-easy axis but in the easy plane of a sublattice). There is no magnetic saturation in the $M(H)$ for fields that are not aligned within the easy plane of either sublattice in the systems (green line).

2. *Monte Carlo simulations*

To confirm the values of J and D, determined using Eqs. (4) and (5) and reported in Table II, classical MC simulations of the powder-averaged $M(H)$ were carried out. $M(H)$ curves were calculated for 100 different field directions evenly spaced on a unit sphere and averaged to calculate the powder averaged $M(H)$. The resulting simulated $M(H)$ curves for $X =$ Cl and Br are shown in Figs. 3(a) and 3(b), respectively, and the differential susceptibilities are shown in Figs. 3(c) and 3(d).

In both $X =$ Cl and Br, there is a good agreement between the experimental and the simulated $M(H)$ curves. The simulations show a small overestimation of the $M(H)$ due to the slight concavity in the measured $M(H)$ curves. In $[Ni(HF_2)(pyz)_2]SbF_6$, a similar discrepancy was attributed to the development of quantum fluctuations resulting from the quasi-one-dimensional nature of the magnetic exchange [4]. Here the discrepancy may also arise from quantum fluctuations in these $S = 1$ systems.

For $X =$ Br, there is a good agreement between simulated and observed $\mu_0 H_{SF}$ and $\mu_0 H_{c1}$. For $X =$ Cl, the larger D/nJ results in a slight underestimation of D when calculated using Eq. (5), which is derived under the approximation that $D \ll nJ$. Consequently, MC simulations using the calculated J and D values (as reported in Table II) results in a slightly smaller simulated $\mu_0 H_{SF}$ than the observed value for $X =$ Cl. However, as seen in Figs. 3(a) and 3(c), the deviation in $\mu_0 H_{SF}$ is small and the derived value of D is expected to be correct within the experimental error.

TABLE II. The AFM exchange energy J and the easy-plane single-ion anisotropy parameter D, derived using mean-field calculations of the observed critical fields in the magnetization $M(H)$ data. The g-factors are the low-temperature values determined experimentally through the $M(H)$ saturation value.

	J (K)	D (K)	g	D/J
$NiCl_2(pym)_2$	8.1(5)	2.6(5)	2.06	0.32(6)
$NiBr_2(pym)_2$	9.2(2)	1.2(3)	2.25	0.13(3)

It is often the case that for anisotropic magnets, a symmetry-breaking phase transition occurs at saturation when a sufficiently large magnetic field is applied along the principle anisotropy axes. In our systems, the rotational symmetry around the SIA axis is broken by the alternation of the Ni(II) octahedra. As a result, field directions perpendicular to the pseudo-easy axis exist for which a phase transition is absent at finite fields. Here, the SIA can always save energy by canting spins away from the applied field and a spin-polarized phase is only reached in the limit of infinite field. This is illustrated by the MC simulation of $M(H)$ for $\mathbf{H}||[1\,0\,0]$ presented in Fig. 8, in which $M(H)$ asymptotically approaches the saturation value. When the applied field is parallel to the pseudo-easy axis, the field-polarized phase minimizes the SIA energy for spin in both i and j sites resulting in the first saturation phase transition at $\mu_0 H_{c1}$. A second saturation field is expected to occur for $\mathbf{H}||[1\,1\,0]$ or $[\bar{1}\,1\,0]$, corresponding to direction in which the field aligns parallel to the hard axis of one site and also within the easy plane of the other site [43]. In a powder-averaged $M(H)$ experiment, the second saturation field is hard to define in the data.

III. CONCLUSION

In summary, we thoroughly characterized the magnetic properties of the $S = 1$ diamond-lattice systems, $NiX_2(pym)_2$ ($X =$ Cl or Br). The octahedral orientation and the SIA axis of neighboring Ni(II) ions connected by AFM exchange-mediating pym ligands alternate by a 90° rotation about the

[0 0 1] direction. While an alternating easy axis induces a spin-canted magnetic order, as seen in $FeCl_2(pym)_2$ [31], $NiCl_2(pym)$, and $NiCl_2(btd)$ [33], an alternating easy-plane anisotropy is expected to result in collinear order along the unique direction created by the intersection of the two easy planes. Here we denote this direction as the pseudo-easy axis. Recent studies on $FeCl_2(pym)$ and $FeCl_2(btd)$ found that while hosting an alternating easy-plane anisotropy, significant spin-canting arose due to rhombic anisotropy, DM or higher-order interaction [32]. In contrast, our neutron diffraction measurements revealed that the magnetic moments in $NiCl_2(pym)_2$ align collinearly along [0 0 1], the pseudo-easy axis.

Similar $\chi(T)$ and a low-field feature in $M(H)$, which is ascribed to a spin-flop transition, was observed in both $X =$ Cl and Br compounds, implying that $X =$ Br also hosted a pseudo-easy-axis anisotropy and adopts the same collinear order. Mean-field calculations of the spin-flop and the magnetization saturation field were used to determine that $J = 8.1(5)$ K, $D = 2.6(5)$ K for $X =$ Cl and $J = 9.2(2)$ K, $D = 1.2(3)$ K for $X =$ Br. The values of J calculated here are comparable to $J = 7$ K reported in Ref. [32] and MC simulations of the powder-average $M(H)$ simulations were performed to verify these Hamiltonian parameters. Moreover, MC simulations of single-crystal $M(H)$ curves indicate that when the applied field is parallel to the pseduo-easy axis, characteristic spin-flop and a magnetic saturation phase-transition, akin to conventional easy-axis systems, occur. However, due to the broken rotational symmetry around the pseduo-easy axis, there are field directions perpendicular to the pseduo-easy axis where the $M(H)$ exhibits an asymptotic approach to magnetic saturation rather than a saturation phase transition at finite fields.

The reduction in D and an increase in secondary exchange through the halide-halide bond in $X =$ Br is in keeping with the magnetostructural correlations established for halides of different radii in $NiX_2(3,5\text{-lut})_4$ [17]. Similar to $NiI_2(3,5\text{-lut})_4$, we expect $NiI_2(pym)_2$ to exhibit a small easy-axis D accompanied by a larger halide-halide exchange interaction. This would lead to the observation of a SIA-induced spin-canted magnetic order, similar to that observed in isostructural $FeCl_2(pym)_2$ [31].

Data presented in this paper will be made available at [49].

ACKNOWLEDGMENTS

We are indebted to the late Jamie Manson for instigating this work, for his role in designing and growing the samples, and for many other invaluable contributions. We thank T. Orton and P. Ruddy for technical assistance. S.V. thanks the EPSRC (UK) for support. This project has received funding from the European Research Council (ERC) under the European Union's Horizon 2020 research and innovation program (Grant Agreement No. 681260). A portion of this work was performed at the National High Magnetic Field Laboratory, which is supported by National Science Foundation Cooperative Agreements No. DMR-1644779 and No. DMR-2128556, the US Department of Energy (DoE), and the State of Florida. J.S. acknowledges support from the DoE BES FWP "Science of 100 T". A.H.M. thanks the STFC and EPSRC for supporting his studentship. Part of this work was carried out at the Swiss Muon Source, Paul Scherrer Institut and we are grateful for the provision of beamtime. The authors also thank the EPSRC for funding (EP/X014606/1, A National Electron Diffraction Facility for Nanomaterial Structural Studies), and the University of Warwick X-Ray Research Technology Platform for the provision of further analysis facilities.

[1] D. C. Dender, P. R. Hammar, D. H. Reich, C. Broholm, and G. Aeppli, Direct observation of field-induced incommensurate fluctuations in a one-dimensional $S = 1/2$ antiferromagnet, Phys. Rev. Lett. **79**, 1750 (1997).

[2] T. Hong, M. Kenzelmann, M. M. Turnbull, C. P. Landee, B. D. Lewis, K. P. Schmidt, G. S. Uhrig, Y. Qiu, C. Broholm, and D. Reich, Neutron scattering from a coordination polymer quantum paramagnet, Phys. Rev. B **74**, 094434 (2006).

[3] V. S. Zapf, D. Zocco, B. R. Hansen, M. Jaime, N. Harrison, C. D. Batista, M. Kenzelmann, C. Niedermayer, A. Lacerda, and A. Paduan-Filho, Bose-Einstein condensation of $S = 1$ nickel spin degrees of freedom in $NiCl_2$-4SC$(NH_2)_2$, Phys. Rev. Lett. **96**, 077204 (2006).

[4] J. Brambleby, J. L. Manson, P. A. Goddard, M. B. Stone, R. D. Johnson, P. Manuel, J. A. Villa, C. M. Brown, H. Lu, S. Chikara, V. Zapf, S. H. Lapidus, R. Scatena, P. Macchi, Y.-S. Chen, L.-C. Wu, and J. Singleton, Combining microscopic and macroscopic probes to untangle the single-ion anisotropy and exchange energies in an $S = 1$ quantum antiferromagnet, Phys. Rev. B **95**, 134435 (2017).

[5] R. C. Williams, W. J. A. Blackmore, S. P. M. Curley, M. R. Lees, S. M. Birnbaum, J. Singleton, B. M. Huddart, T. J. Hicken, T. Lancaster, S. J. Blundell, F. Xiao, A. Ozarowski, F. L. Pratt, D. J. Voneshen, Z. Guguchia, C. Baines, J. A. Schlueter, D. Y. Villa, J. L. Manson, and P. A. Goddard, Near-ideal molecule-based Haldane spin chain, Phys. Rev. Res. **2**, 013082 (2020).

[6] A. E. Thorarinsdottir and T. D. Harris, Metal–organic framework magnets, Chem. Rev. **120**, 8716 (2020).

[7] E. Coronado, Molecular magnetism: From chemical design to spin control in molecules, materials and devices, Nat. Rev. Mater. **5**, 87 (2020).

[8] N. F. Chilton, Molecular magnetism, Annu. Rev. Mater. Res. **52**, 79 (2022).

[9] P. A. Goddard, J. L. Manson, J. Singleton, I. Franke, T. Lancaster, A. J. Steele, S. J. Blundell, C. Baines, F. L. Pratt, R. D. McDonald, O. E. Ayala-Valenzuela, J. F. Corbey, H. I. Southerland, P. Sengupta, and J. A. Schlueter, Dimensionality selection in a molecule-based magnet, Phys. Rev. Lett. **108**, 077208 (2012).

[10] J. Pitcairn, A. Iliceto, L. Cañadillas-Delgado, O. Fabelo, C. Liu, C. Balz, A. Weilhard, S. P. Argent, A. J. Morris, and M. J. Cliffe, Low-dimensional metal–organic magnets as a route toward the $S = 2$ Haldane phase, J. Am. Chem. Soc. **145**, 1783 (2023).

[11] Y. Wang, P. Fu, H. Takatsu, C. Tassel, N. Hayashi, J. Cao, T. Bataille, H.-J. Koo, Z. Ouyang, M.-H. Whangbo, H. Kageyama, and H. Lu, Construction of ideal one-dimensional spin chains by topochemical dehydration/rehydration route, J. Am. Chem. Soc. **146**, 8320 (2024).

[12] J. A. Schlueter, H. Park, G. J. Halder, W. R. Armand, C. Dunmars, K. W. Chapman, J. L. Manson, J. Singleton, R. McDonald, A. Plonczak *et al.*, Importance of halogen halogen contacts for the structural and magnetic properties of CuX_2 (pyrazine-N, N'-dioxide)$(H_2O)_2$ (X = Cl and Br), Inorg. Chem. **51**, 2121 (2012).

[13] M. Cortijo, S. Herrero, R. Jimenez-Aparicio, and E. Matesanz, Modulation of the magnetic properties of two-dimensional compounds [NiX_2(N–N)] by tailoring their crystal structure, Inorg. Chem. **52**, 7087 (2013).

[14] M. Cortijo, S. Herrero, R. Jimenez-Aparicio, J. Perles, J. L. Priego, and J. Torroba, Tuning of adsorption and magnetic properties in a series of self-templated isostructural Ni(II) metal-organic frameworks, Cryst. Growth Des. **14**, 716 (2014).

[15] J. Liu, P. A. Goddard, J. Singleton, J. Brambleby, F. Foronda, J. S. Möller, Y. Kohama, S. Ghannadzadeh, A. Ardavan, S. J. Blundell *et al.*, Antiferromagnetism in a family of $S = 1$ square lattice coordination polymers NiX_2(pyz)$_2$ (X = Cl, Br, I, NCS; pyz=pyrazine), Inorg. Chem. **55**, 3515 (2016).

[16] M. Kubus, A. Lanza, R. Scatena, L. H. Dos Santos, B. Wehinger, N. Casati, C. Fiolka, L. Keller, P. Macchi, C. Ruegg *et al.*, Quasi-2d Heisenberg antiferromagnets [CuX(pyz)$_2$](BF$_4$) with X = Cl and Br, Inorg. Chem. **57**, 4934 (2018).

[17] W. J. A. Blackmore, S. P. M. Curley, R. C. Williams, S. Vaidya, J. Singleton, S. Birnbaum, A. Ozarowski, J. A. Schlueter, Y.-S. Chen, B. Gillon, A. Goukassov, I. Kibalin, D. Y. Villa, J. A. Villa, J. L. Manson, and P. A. Goddard, Magneto-structural correlations in Ni^{2+}–Halide$\cdots$Halide–Ni^{2+} chains, Inorg. Chem. **61**, 141 (2022).

[18] M. Geers, J. Y. Lee, S. Ling, O. Fabelo, L. Cañadillas-Delgado, and M. J. Cliffe, Non-collinear magnetism in the post-perovskite thiocyanate frameworks CsM(NCS)$_3$, Chem. Sci. **14**, 3531 (2023).

[19] F. M. Woodward, P. J. Gibson, G. B. Jameson, C. P. Landee, M. M. Turnbull, and R. D. Willett, Two-dimensional heisenberg antiferromagnets: Syntheses, x-ray structures, and magnetic behavior of [Cu(pz)$_2$](ClO$_4$)$_2$, [Cu(pz)$_2$](BF$_4$)$_2$, and [Cu(pz)$_2$(NO$_3$)](PF$_6$), Inorg. Chem. **46**, 4256 (2007).

[20] J. L. Manson, S. H. Lapidus, P. W. Stephens, P. K. Peterson, K. E. Carreiro, H. I. Southerland, T. Lancaster, S. J. Blundell, A. J. Steele, P. A. Goddard *et al.*, Structural, electronic, and magnetic properties of quasi-1d quantum magnets [Ni(HF$_2$)(pyz)$_2$]X (pyz= pyrazine; X = PF$_6^-$, SbF$_6^-$) Exhibiting Ni-FHF-Ni and Ni-pyz-Ni spin interactions, Inorg. Chem. **50**, 5990 (2011).

[21] D. M. Pajerowski, A. P. Podlesnyak, J. Herbrych, and J. Manson, High-pressure inelastic neutron scattering study of the anisotropic s=1 spin chain [Ni(HF$_2$)(3-Clpyridine)$_4$]BF$_4$, Phys. Rev. B **105**, 134420 (2022).

[22] M. J. Coak, S. P. M. Curley, Z. Hawkhead, J. P. Tidey, D. Graf, S. J. Clark, P. Sengupta, Z. E. Manson, T. Lancaster, P. A. Goddard, and J. L. Manson, Asymmetric phase diagram and dimensional crossover in a system of spin-$\frac{1}{2}$ dimers under applied hydrostatic pressure, Phys. Rev. B **108**, 224431 (2023).

[23] M. Geers, D. M. Jarvis, C. Liu, S. S. Saxena, J. Pitcairn, E. Myatt, S. A. Hallweger, S. M. Kronawitter, G. Kieslich, S. Ling, A. B. Cairns, D. Daisenberger, O. Fabelo, L. Cañadillas-Delgado, and M. J. Cliffe, High-pressure behavior of the magnetic van der Waals molecular framework Ni(NCS)$_2$, Phys. Rev. B **108**, 144439 (2023).

[24] K. Y. Povarov, D. E. Graf, A. Hauspurg, S. Zherlitsyn, J. Wosnitza, T. Sakurai, H. Ohta, S. Kimura, H. Nojiri, V. O. Garlea *et al.*, Pressure-tuned quantum criticality in the large-D antiferromagnet DTN, Nat. Commun. **15**, 2295 (2024).

[25] R. Feyerherm, S. Abens, D. Günther, T. Ishida, M. Meißner, M. Meschke, T. Nogami, and M. Steiner, Magnetic-field induced gap and staggered susceptibility in the $S = 1/2$ chain [PMCu(NO$_3$)$_2$(H$_2$O)$_2$]$_n$ (PM= pyrimidine), J. Phys.: Condens. Matter **12**, 8495 (2000).

[26] S. A. Zvyagin, A. K. Kolezhuk, J. Krzystek, and R. Feyerherm, Excitation hierarchy of the quantum sine-gordon spin chain in a strong magnetic field, Phys. Rev. Lett. **93**, 027201 (2004).

[27] J. Liu, S. Kittaka, R. D. Johnson, T. Lancaster, J. Singleton, T. Sakakibara, Y. Kohama, J. van Tol, A. Ardavan, B. H. Williams, S. J. Blundell, Z. E. Manson, J. L. Manson, and P. A. Goddard, Unconventional field-induced spin gap in an $S = 1/2$ chiral staggered chain, Phys. Rev. Lett. **122**, 057207 (2019).

[28] B. M. Huddart, M. Gomilšek, T. J. Hicken, F. L. Pratt, S. J. Blundell, P. A. Goddard, S. J. Kaech, J. L. Manson, and T. Lancaster, Magnetic order and ballistic spin transport in a sine-Gordon spin chain, Phys. Rev. B **103**, L060405 (2021).

[29] M. Oshikawa and I. Affleck, Field-induced gap in $S = 1/2$ antiferromagnetic chains, Phys. Rev. Lett. **79**, 2883 (1997).

[30] I. Affleck and M. Oshikawa, Field-induced gap in cu benzoate and other $S = \frac{1}{2}$ antiferromagnetic chains, Phys. Rev. B **60**, 1038 (1999).

[31] R. Feyerherm, A. Loose, T. Ishida, T. Nogami, J. Kreitlow, D. Baabe, F. J. Litterst, S. Süllow, H.-H. Klauss, and K. Doll, Weak ferromagnetism with very large canting in a chiral lattice: Fe(pyrimidine)$_2$Cl$_2$, Phys. Rev. B **69**, 134427 (2004).

[32] J. Kreitlow, D. Menzel, A. U. B. Wolter, J. Schoenes, S. Süllow, R. Feyerherm, and K. Doll, Pressure dependence of $C_4N_2H_4$-mediated superexchange in XCl$_2$($C_4N_2H_4$)$_2$ (X = Fe, Co, Ni), Phys. Rev. B **72**, 134418 (2005).

[33] J. Pitcairn, M. A. Ongkiko, A. Iliceto, P. J. Speakman, S. Calder, M. J. Cochran, J. A. M. Paddison, C. Liu, S. P. Argent, A. J. Morris, and M. J. Cliffe, Controlling noncollinear ferromagnetism in van der Waals metal–organic magnets, J. Am. Chem. Soc. **146**, 19146 (2024).

[34] K. Y. Povarov, L. Facheris, S. Velja, D. Blosser, Z. Yan, S. Gvasaliya, and A. Zheludev, Magnetization plateaux cascade in the frustrated quantum antiferromagnet Cs_2CoBr_4, Phys. Rev. Res. **2**, 043384 (2020).

[35] L. Facheris, S. D. Nabi, K. Y. Povarov, Z. Yan, A. G. Moshe, U. Nagel, T. Rõõm, A. Podlesnyak, E. Ressouche, K. Beauvois, J. R. Stewart, P. Manuel, D. Khalyavin, F. Orlandi, and A. Zheludev, Magnetic field induced phases and spin Hamiltonian in Cs_2CoBr_4, Phys. Rev. B **109**, 104433 (2024).

[36] See Supplemental Material at http://link.aps.org/supplemental/10.1103/PhysRevB.110.174438 for further details on experimental methods, calculations, and additional crystal structure and magnetometry data. A magnetic cif file containing the

magnetic structure of $NiCl_2(pym)_2$ is also provided. The Supplemental Material also contains Refs. [44–48].

[37] M. E. Fisher, Relation between the specific heat and susceptibility of an antiferromagnet, Philos. Mag. **7**, 1731 (1962).

[38] *Muon Spectroscopy: An Introduction*, edited by S. J. Blundell, R. D. Renzi, T. Lancaster, and F. L. Pratt (Oxford University Press, Oxford, 2022).

[39] L. C. Chapon, P. Manuel, P. G. Radaelli, C. Benson, L. Perrott, S. Ansell, N. J. Rhodes, D. Raspino, D. Duxbury, E. Spill *et al.*, Wish: The new powder and single crystal magnetic diffractometer on the second target station, Neutron News **22**, 22 (2011).

[40] J. Rodríguez-Carvajal, Recent advances in magnetic structure determination by neutron powder diffraction, Phys. B: Condens. Matter **192**, 55 (1993).

[41] H. T. Stokes, D. M. Hatch, and B. J. Campbell, ISODISTORY, ISOTROPY Software Suite, iso.byu.edu.

[42] B. J. Campbell, H. T. Stokes, D. E. Tanner, and D. M. Hatch, Isodisplace: A web-based tool for exploring structural distortions, J. Appl. Cryst. **39**, 607 (2006).

[43] The hard axis of one site aligns within the easy plane of the second site because of the exact 90° rotation of the Ni(II) between neighboring sites. For rotation by an angle which is not a multiple of 90°, saturation phase transitions will not occur for any directions perpendicular to the pseudo-easy axis.

[44] L. J. Bourhis, O. V. Dolomanov, R. J. Gildea, J. A. Howard, and H. Puschmann, The anatomy of a comprehensive constrained, restrained refinement program for the modern computing environment–Olex2 dissected, Acta Cryst. A **71**, 59 (2015).

[45] G. M. Sheldrick, Crystal structure refinement with *SHELXL*S, Acta Cryst. C **71**, 3 (2015).

[46] O. V. Dolomanov, L. J. Bourhis, R. J. Gildea, J. A. Howard, and H. Puschmann, Olex2: A complete structure solution, refinement and analysis program, J. Appl. Cryst. **42**, 339 (2009).

[47] A. Saha, S. S. Nia, and J. A. Rodríguez, Electron diffraction of 3D molecular crystals, Chem. Rev. **122**, 13883 (2022).

[48] P. B. Klar, Y. Krysiak, H. Xu, G. Steciuk, J. Cho, X. Zou, and L. Palatinus, Accurate structure models and absolute configuration determination using dynamical effects in continuous-rotation 3D electron diffraction data, Nat. Chem. **15**, 848 (2023).

[49] https://wrap.warwick.ac.uk/188216/.